Table of Content

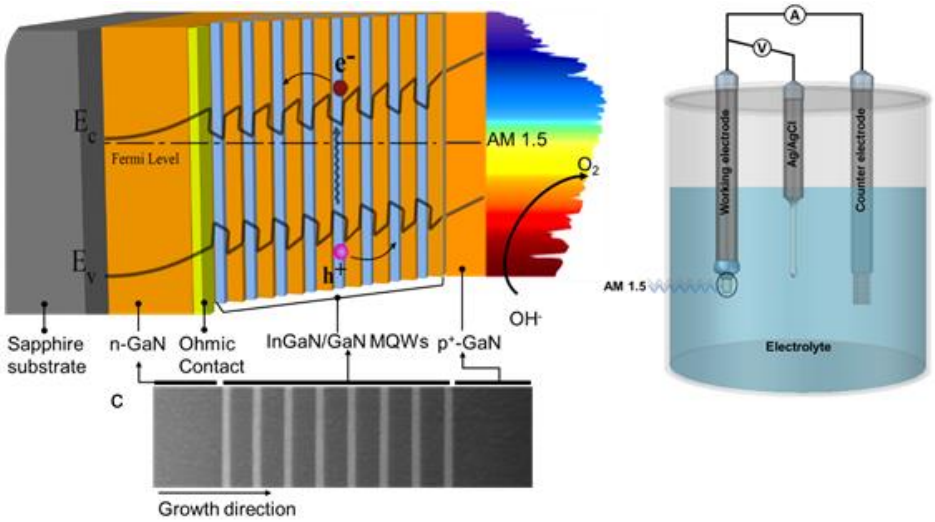

InGaN/GaN Multiple Quantum Well Photoanode Modified with Cobalt Oxide for Water Oxidation

Mahdi Alqahtani*¶‡, Sanjayan Sathasivam§, Abdullah Alhassen‡,∥, Fan Cui¶, Sultan BenJaber§, Chris Blackman§, Bin Zhang⊥, Yong Qin⊥, Ivan Parkin§, Shuji Nakamura ∥, Huiyun Liu*¶, and Jiang Wu*¶

† Department of Electronic and Electrical Engineering, University College London, London, United Kingdom

‡ King Abdulaziz City for Science and Technology, Saudi Arabia

§ Department of Chemistry, University College London, London, United Kingdom

A. Alhassen, S. Nakamura

∥Materials Department, University of California, Santa Barbara, United States of America

⊥ Institute of Coal Chemistry, Chinese Academy of Sciences, China

Abstract Indium gallium nitride (InGaN) is an attractive semiconductor, with a tunable direct bandgap for photoelectrochemical water splitting, but it corrodes in aqueous electrolytes. Cobalt oxide (CoO_x) is a promising co-catalyst to protect photoelectrodes and to accelerate the charge transfer. CoO_x is earth-abundant and stable in extremely alkaline conditions and shows high activity for the oxygen evolution reaction (OER). In this work, we demonstrate that CoO_x directly deposited onto InGaN/GaN multiple quantum wells photoanodes exhibits excellent activity and stability in a strong alkaline electrolyte, 1M NaOH (pH=13.7), for water oxidation up to 28 hours, while a reference sample without the catalyst degraded rapidly in the alkaline electrolyte. Under simulated solar illumination, the CoO_x-modified InGaN/GaN quantum well photoanode showed a high photocurrent density of 1.26 mA cm^{-2} at 1.23 V and an onset potential of -0.03 V versus a reversible hydrogen electrode.

Keywords: indium gallium nitrides; quantum wells; photoelectrochemical water splitting; photoanodes; cobalt oxides

Introduction

Since the burning of petroleum derivatives (coal, gaseous petrol, and oil) represents most carbon emissions, renewable energy sources, for example, solar energy, are viewed as desperately required solutions for energy and the environment.[1,2] Photoelectrochemical (PEC) water splitting is a promising method to harvest solar energy and can provide clean energy (e.g., hydrogen); it converts sunlight directly to hydrogen by cleaving water molecules.[3,4] Fujishima and Honda's 1972 discovery of PEC water splitting by titanium dioxide (TiO_2) under ultraviolet radiation led to intensive research in this field, but critical challenges remain.[5] For instance, metal oxides (e.g., TiO_2) are resistant to corrosion but have a lower visible light absorption efficiency and slow charge transport kinetics, which are limitations to achieving high solar-to-hydrogen conversion efficiency.[5] On the other hand, PEC electrodes, based on III-V semiconductors used for water oxidation exhibited high performance owing to their excellent optical properties in the visible region of the electromagnetic spectrum, but they are thermodynamically unstable and corrode rapidly in aqueous electrolytes.[6-8] Therefore, efficient and stable photoanodes are crucial to accomplishing long-term economic hydrogen production by PEC water splitting due to the shortage of stable oxygen evolution reaction (OER) catalysts.[9] Group III-nitride semiconductors, for example, indium gallium nitride (InGaN), have recently become promising candidates for PEC water splitting because they have a tunable direct bandgap from the ultraviolet to the near-infrared range covering the entire solar spectrum[10,11] and widely used in optoelectronic and electronic applications.[12] Moreover, their conduction and valence band edges straddle the hydrogen reduction (H^+/H_2) and water oxidation (H_2O/O_2) potentials.[11] In the recent years, extensive studies have investigated InGaN and GaN photoelectrodes but yet with limited success.[13-17] For instance, a InGaN NW photoanode modified with Iridium oxide (IrO_2) co-catalyst exhibited a high photocurrent

density under illumination but corroded rapidly in solution.[18] Very recently, Co_3O_4 nano-islands were shown to reduce the onset potential and improve the stability of a GaN NW photoanode[19]. However, the nano-islands lead to an incomplete coverage of the catalyst over the GaN surface and hence limited stability in a strong alkaline electrolyte. Moreover, Co-Pi-modified GaN photoaonde has shown some improvement in the onset potential and the photocurrent but poor resistance against photocorrosion[16]. Moreover, the growth of high quality of InGaN photoanode with a high indium content is rather difficult due to the lattice mismatch between GaN and InN.[12,20] To overcome these limitations, InGaN/GaN multiple quantum wells (MQWs) with suitable surface modification may be adopted to achieve stable and efficient PEC water splitting.

In the present study, we demonstrate a high-quality InGaN/GaN MQW photoanode modified with cobalt oxide using atomic layer deposition (ALD). The surface coating improved the photocurrent due to reduced overpotential, resulting in a stable photocurrent of the InGaN/GaN MQWs photoanode in an alkaline electrolyte (1M NaOH, pH 13.7) for up to 28 hr. Moreover, the InGaN/GaN MQWs photoanode modified with CoO_x produced a low onset potential of - 0.03 V and a high photocurrent density of 1.26 mA cm^{-2} versus RHE while the InGaN/GaN MQWs without any co-catalyst showed a reduced photocurrent of 0.94 mA cm^{-2} and onset potential 0.01 V at potential 1.23 V versus RHE, respectively. Electrochemical impedance spectroscopy confirmed that the coupling of CoO_x onto InGaN/GaN MQWs reduced the electrochemical reaction resistance to some extent and thus enhanced the stability of InGaN/GaN MQWs for water oxidation.

Results and discussion

High-quality InGaN/GaN MQWs photoanode for PEC water splitting were grown heteroepitaxially by atmospheric pressure metal organic chemical vapour deposition

(MOCVD) on (0001) patterned sapphire substrates (PSS). A suitably high active co-catalyst for the oxygen evolution reaction (OER) was required to stabilize a photoelectrode in high pH solution and promote charge transfer. Earth-abundant cobalt oxide was chosen as the OER co-catalyst for InGaN/GaN MQWs photoanode. The CoO_x catalyst has excellent hole conduction and electron blocking properties due to its high conduction edge position, particularly under strong alkaline conditions.[21] The CoO_x catalyst was directly deposited onto the InGaN/GaN MQWs' surface using atomic layer deposition (ALD) and has been shown to enhance the stability of photoanodes[22,23].

A schematic of an InGaN/GaN MQWs photoanode and experimental setup are shown in Figure 1a-c. Eight stacks of InGaN/GaN MQWs epitaxially grown on (0001) sapphire substrates were employed for photoanodic water splitting. InGaN/GaN MQWs allow additional photon absorption in the visible region.

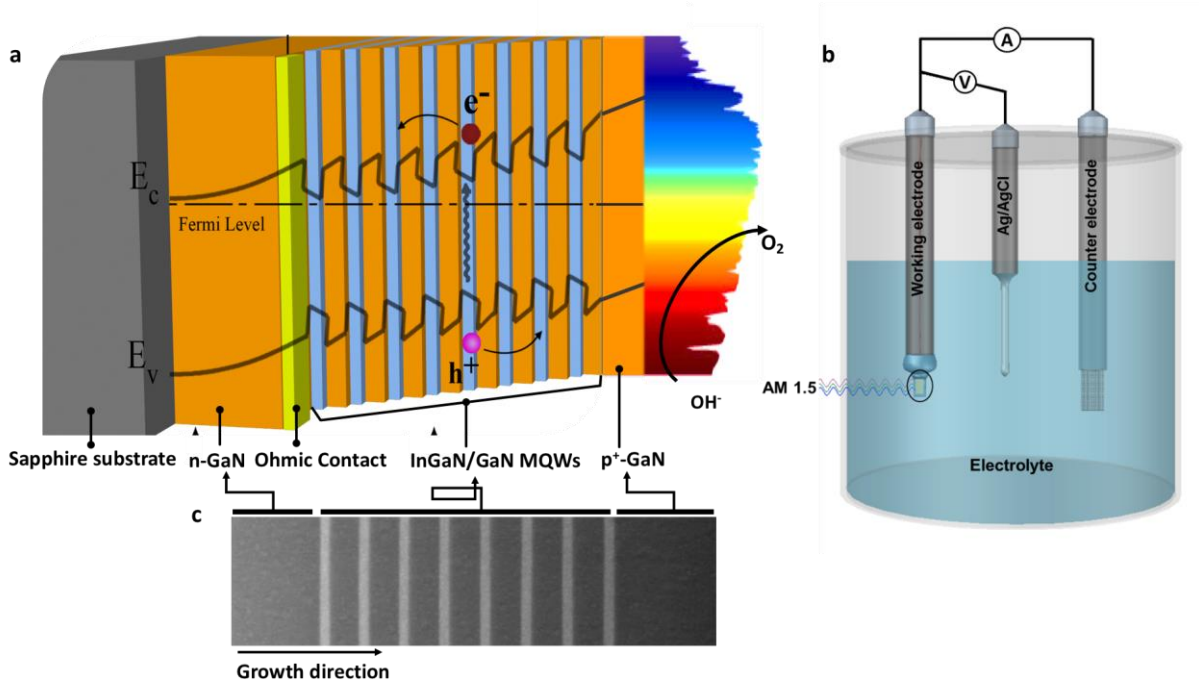

Figure 1. (a) Schematic of InGaN/GaN MQWs photoanode structure were grown by MOCVD on (0001) patterned sapphire substrates (PSS) then by a GaN buffer 3.5 μm followed by the active region consisted of an undoped eight periods -quantum wells (MQW). The Schematic is illustration of the general concept of single photoelectrode under an AM 1.5G illumination, incoming photons (hv) generate electrons (e^-) and holes (h^+) pairs in the active region where they will be separated by internal electric field. The holes move toward semiconductor/electrolyte interface to drive the OER and the electrons are moved toward the rear ohmic contact and through an electrical connection to the surface of the counter electrode to drive the HER. (b) A schematic diagram of the experimental setup used for the photoelectrochemical measurements which consists of the working electrode (InGaN/GaN MQWs), reference electrode (Ag/AgCl), and counter electrode (platinum coil). (c) The TEM cross-section shows the InGaN/GaN MQWs photoanode and its growth direction.

The structural properties of InGaN/GaN MQWs were analysed by scanning transmission electron microscopy (STEM). The low-magnification TEM images in Figure 2a (see Figure S1 and S2 in supporting information) show that the active region is virtually free of any dislocations. Figure 2b shows high-resolution TEM images of the

eight quantum wells, which unambiguously show defect-free single crystalline epilayers. A lattice constant of about 0.52 nm was measured for both InGaN wells (~3 nm) and GaN barriers (~10 nm), indicating coherent strained InGaN quantum wells on the GaN (0001) surface. Each quantum well shows a sharp contrast between wells and barriers, indicating high interface quality with marginal intermixing. No interfacial dislocations or misfits can be observed, although a high indium composition of about 20% was introduced in the wells. Figure 2c shows the fast Fourier transform of the high-resolution TEM images of Figure 2b, which confirms the growth of defect-free MQWs with a pure wurtzite crystal structure. The crystal quality and catalyst layer play a critical role in the STH conversion efficiency of PEC cells because material imperfections are the major contribution to nonradiative recombination and are detrimental to photo-excited carriers for H_2 and O_2 evolution reactions. Although one-dimensional nanomaterials are capable of accommodating the materials of large lattice mismatches, it has been shown that various types of dislocations (e.g., stacking faults) as well as a high density of surface states largely undermine the performance of nanowire or nanorod devices. Therefore, high crystal quality of MQWs may serve as good alternative to one-dimensional nanostructures for high indium content InGaN PEC cells.

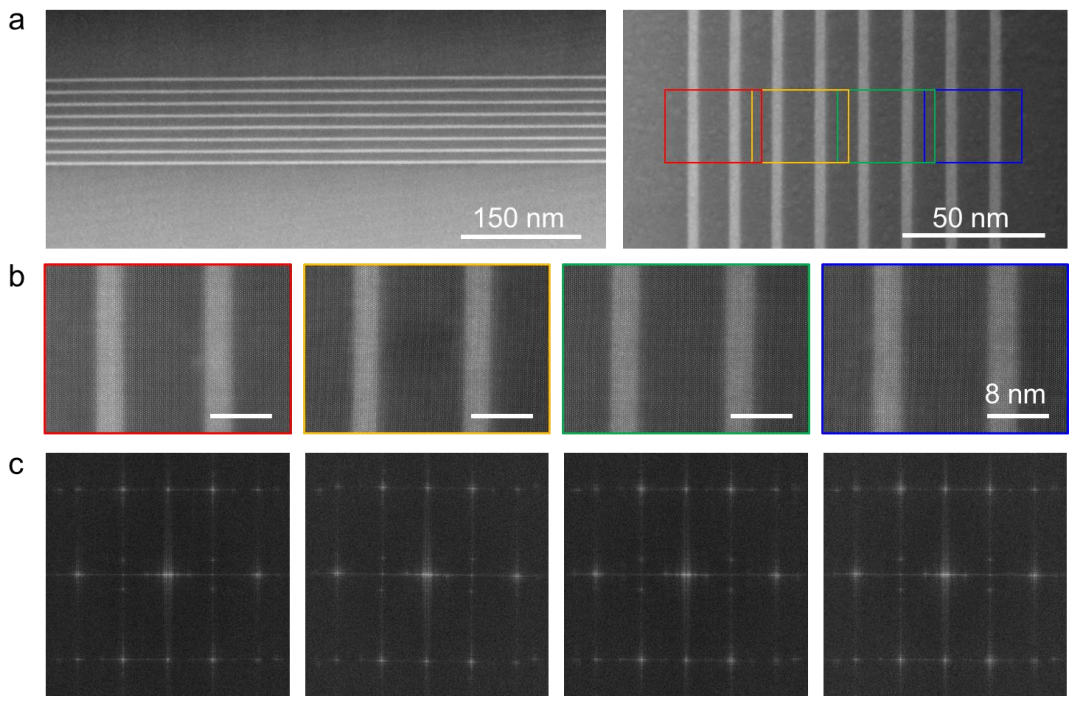

Figure 2. Structural characterization of InGaN/GaN MQWs photoanode. (a) The high resolution TEM images of InGaN/GaN MQWs photoanode which show that the structure is virtually free of any dislocations. (b) TEM images of eight quantum wells showing defect-free single crystalline epilayers. (c) Fast Fourier transform of the high-resolution images of Fig. 2b.

STEM energy dispersive X-ray spectroscopy (EDS) measurements were carried out to extract the indium content in the QWs. An EDS line scan across the QWs showed that they were highly uniform in indium composition, with all showing a uniform indium composition of around 20% or an atomic percentage of 10% (see Figure 3a). As shown in Figure 3b, EDS elemental mapping also offers evidence of the composition uniformity of InGaN QWs. To further investigate the material properties of InGaN/GaN MQWs, X-ray diffraction (XRD) was performed; the XRD pattern of the MQWs is shown Figure 3c. The diffraction peak at zero arc-sec corresponds to the GaN (0002) plane. The XRD pattern from ω-2θ scan exhibits distinct satellite peaks, indicating high interfacial quality between the InGaN QWs and GaN barriers. The period thickness of a pair InGaN QW and GaN barrier is measured at 12.8 nm, which is consistent with

the TEM measurements. The optical properties of InGaN/GaN MQWs were further studied using photoluminescence (PL) spectroscopy, as shown in Figure 3d. The PL emission peak takes place at ~ 519 nm, which corresponds to the emission from InGaN QWs. Furthermore, STEM energy dispersive X-ray spectroscopy (EDS) measurements for the CoOx layer (~ 13 nm) on the top of the p-type GaN layer are shown in Figure 3e-g (and Fig. S3 in supporting information). It shows a highly dense layer composed of only Co and O, shown in orange colour magenta color, respectively. To further confirm surface structure, Raman measurements were carried out using a Renishaw inVia micro-Raman system, with a laser line of 532 nm as shown in Figure S4 a-b (in supporting information). The Raman spectrum of InGaN/GaN MQWs, with an E2 phonon mode of GaN at ≈ 568 cm^{-1}, and the A1 longitudinal optical (LO) phonon mode at ≈ 734 cm^{-1}, was clearly observed, confirming the surface layer of GaN. These observed modes are in agreement with reported values.[24] While the Raman spectrum of InGaN/GaN MQWs-CoOx shows both modes of GaN E2 and A1(LO) being observed, at 568 cm^{-1} and 733 cm^{-1}, respectively, and another peak at ≈ 688 cm^{-1}, which attributed to the CoOx phonons mode, which helps confirm the presence of CoOx in the top layer.

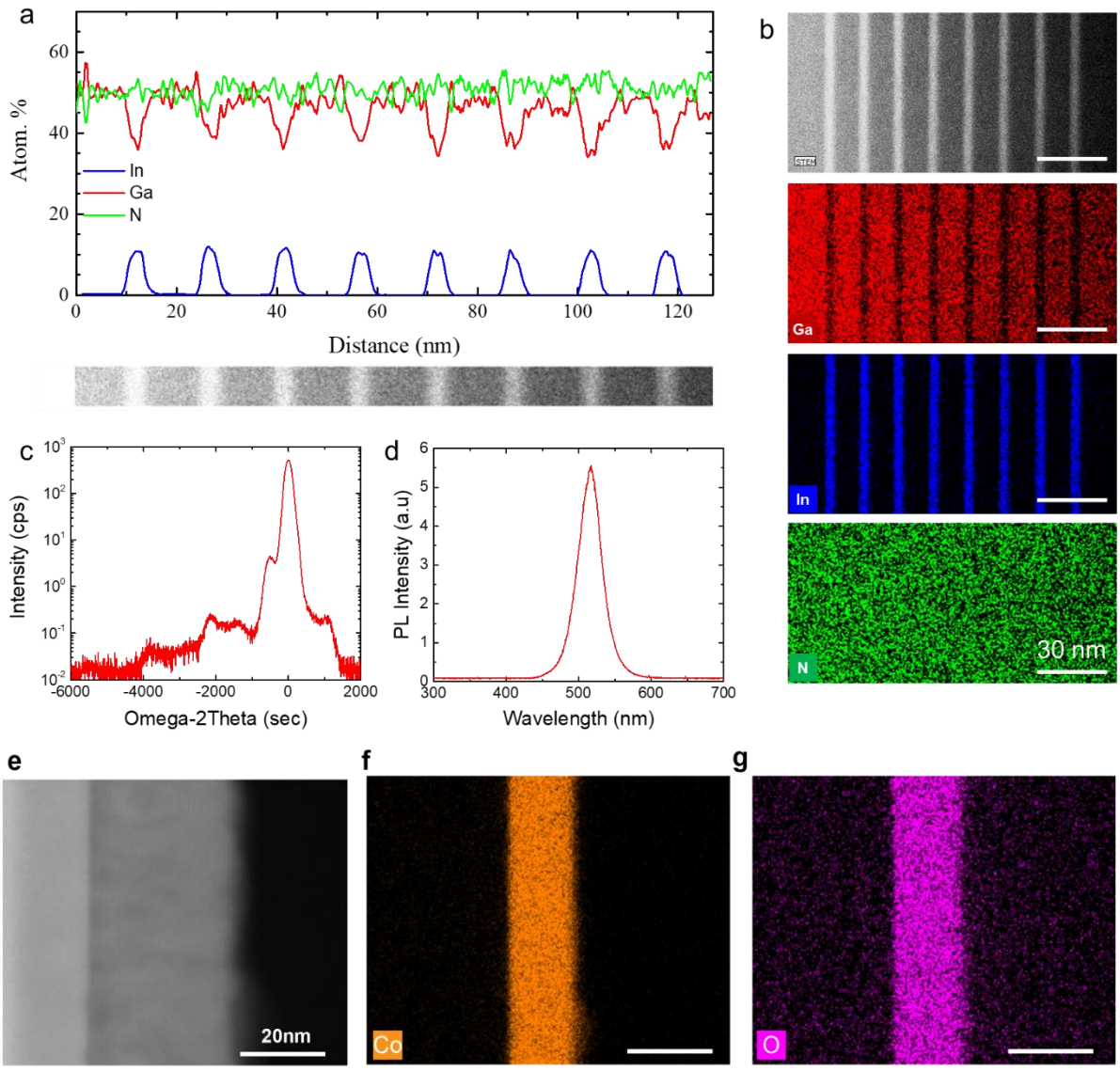

Figure 3. Characterizations of InGaN/GaN MQW-CoOx photoanode. (a) (Color online) In, N, and Ga concentration depth profiles for InGaN/GaN MQW photoanode using STEM energy dispersive X-ray spectroscopy (EDS) measurements. (b) EDS elemental mapping for InGaN/GaN MQWs photoanode showing a good composition uniformity of InGaN QWs. (c) XRD (0002) $\omega/2\theta$ scan measurements of InGaN/GaN MQW photoanode. (d) Photoluminescence spectra of the InGaN/GaN MQW photoanode at room temperature. (e) STEM image of thin layer CoO_x co-catalyst on the surface of p-type GaN layer. (f) and (g) EDS elemental mapping showing CoO_x thin layer to be composed of only Co (orange) and O (magenta).

The PEC performance of InGaN/GaN MQW photoanodes was carried out using a standard three-electrode potentiostatic configuration, including a silver–silver chloride

(Ag/AgCl) reference electrode, a Pt coil counter electrode, and a working electrode in 1 M NaOH electrolyte (pH ~13.7) under 1 sun illumination. The photocurrent density–voltage (*J*–*V*) characteristics are shown in Figure 4a for the bare InGaN/GaN MQW and InGaN/GaN MQW modified with CoO_x. As shown in Figure 4a, the saturated photocurrent of the InGaN/GaN MQW electrode reached ~ 0.95 mA cm^{-2} at a potential 1.23 V versus the reversible hydrogen evolution (RHE). A significant improvement in photocurrent was obtained by using the cobalt oxide as co-catalyst; the saturated photocurrent increased to around 1.26 mA cm^{-2} at a potential 1.23 V versus RHE. Moreover, the onset potentials for the InGaN/GaN MQW and InGaN/GaN MQW modified with CoO_x are 0.01 V and -0.03 V, respectively. The significant anodic shift can be attributed to improved carrier extraction/collection efficiency and enhanced charge carrier transport at the semiconductor/electrolyte interface when using the cobalt oxide catalyst[19].

The incident photon-to-current conversion efficiency (IPCE) for both photoanodes was further investigated at 1.23 V versus RHE. As shown in Figure 4b, an IPCE of InGaN/GaN MQW-CoO_x at 380 nm is 16.8%, which is higher than the value of the bare InGaN/GaN MQW photoanode (~ 10.3% at 380 nm). The IPCE measurement is consistent with the (*J*–*V*) measurements. The improved IPCE value also indicates efficient carrier separation and collection, or fast charge transfer to semiconductor/electrolyte interface while using CoO_x as co-catalyst. The IPCE value decreases towards longer wavelengths (> 500 nm).

To obtain more insight into charge transfer performance at the semiconductor/electrolyte interface, electrochemical impedance spectra (EIS) measurements were conducted using standard three-electrode configuration in 1 M NaOH electrolyte (PH ~13.7) under dark conditions. The EIS measurement was

obtained in the range of $10\text{kHz} - 3\text{MHz}$ at an amplitude of 10 mV and the equivalent circuit model that was used to fit the EIS data. As shown in Figure S5 (see supporting information), the InGaN/GaN MQW-CoO_x photoanode shows a lower charge transfer resistance and higher conductivity compared to the bare InGaN/GaN MQW photoanode without catalyst, which confirms the improved charge transfer by using high catalytic OER catalyst cobalt oxide.

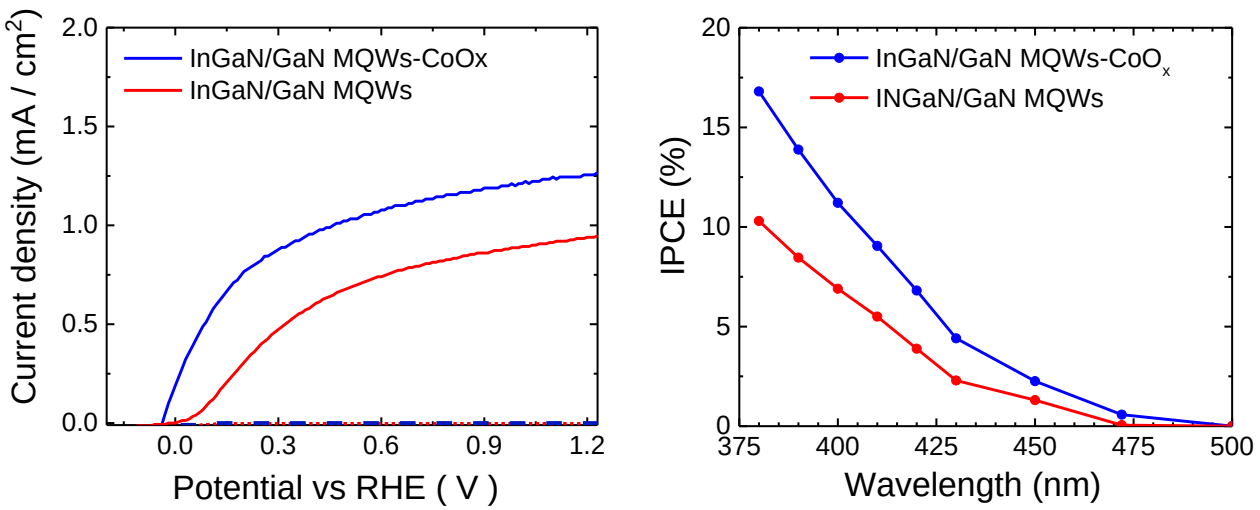

Figure 4. Photoelectrochemical measurements of InGaN/GaN MQW of photoanodes. **(a)** Photocurrent density–potential (*J*–*V*) curves (scan rate is 50 mV s^{-1}) in 1 M NaOH electrolyte under 1 sun illumination versus RHE (V) **(b)** Incident photon-to-current conversion efficiency (IPCE) of InGaN/GaN MQW and InGaN/GaN MQW-CoO_x photoanodes in 1M NaOH electrolyte at 1.23 V versus RHE.

Photoelectrode stability is an essential requirement and an outstanding challenge for PEC cells. The photocurrent density–time (*J*–*t*) characteristics of InGaN/GaN MQW photoanodes were investigated for 28 hr under zero bias in a corrosive solution of 1M NaOH electrolyte (pH ~13.7), as shown in Figure 5a-b. The photocurrent of the bare InGaN/GaN MQW photoanode decreased rapidly at the beginning, which was attributed to significant photocorrosion. On the other hand, the InGaN/GaN MQW

photoanode modified by cobalt oxide shows an initial increase in photocurrent density over the first four hours due to the CoOx catalyst layer assisting in charge transfer and also protecting the InGaN/GaN MQW photoanode against the corrosive electrolyte. Beyond the first four hours the photocurrent density starts to slowily decrease with time due to photocorrosion of the CoOx layer and to some extent the photoanode. However, though decreasing the photocurrent density is still sustained over an extended reaction duration (> 21 hr). While the photocurrent of the bare InGaN/GaN MQW photoanode was degraded to around 0 mA cm^{-2} after only 40 min of experiment, the photocurrent of the InGaN/GaN MQW modified with cobalt oxide was not degraded until extensive PEC reaction (~ 28 hr). Clearly, the catalyst can enhance the stability of the InGaN/GaN MQW photoanode. This is attributed to the CoOx behaving as an effective hole scavenger with electron blocking properties owing to its high conduction edge position that enables it to collect the photogenerated holes away from the photoanode, thus reducing photo-oxidation. This is particularly true under strong alkaline conditions such as here[19 23,25]

To compare the degree of photocorrosion of the two photoanodes, the bare InGaN/GaN MQW after 2 hours of reaction and the modified-CoO_x InGaN/GaN MQW after 28 hours of reaction, the surface morphology of the photoanodes after reaction was studied by scanning electron microscopy (SEM) and X-ray photoelectron spectroscopy (XPS). Figure 5c-d shows the SEM images of the surfaces of the InGaN/GaN MQW-CoO_x and the bare InGaN/GaN MQW photoelectrodes after the stability test. Both photoanodes show different degrees of photocorrosion. The InGaN/GaN MQW-CoO_x photoanode showed a smooth and pinhole-free surface before PEC, as shown in (S3 supporting information), and after PEC, this protective layer was still visible, with only small areas of the film showing the ordered surface textures caused by PEC corrosion of the nitride layers. By contrast, the entire surface

of the bare InGaN/GaN MQW photoanode showed surface textures due to PEC etching, indicating that the photoelectrode was severely corroded.

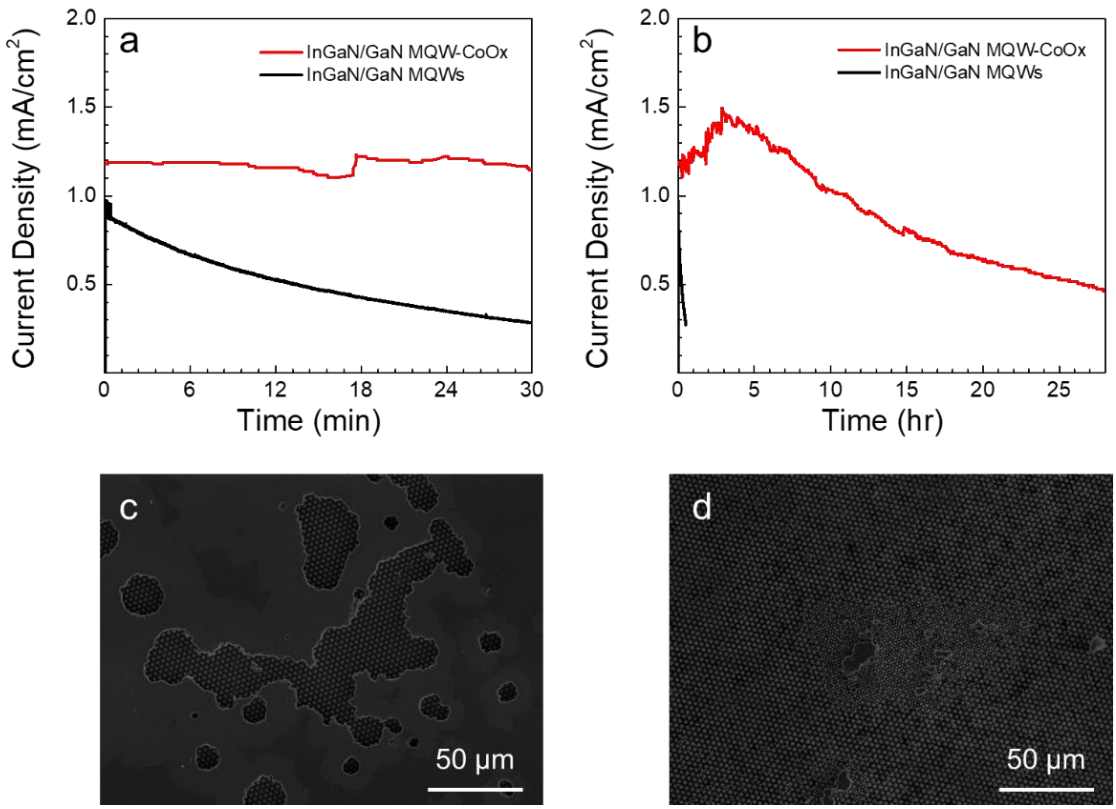

Figure 5. Long-term performances of InGaN/GaN MQW and InGaN/GaN MQW-CoO_x photoanodes**.** (a-b) Current density–time profile of both InGaN/GaN MQW photoanode s at zero bias in 1M NaOH (pH 13.7) versus Pt counter electrode under simulated sunlight using AM1.5G filter for 28 hours. (c) SEM image of InGaN/GaN MQW-CoO_x photoanode after reliability test 28 hours (d) SEM image of InGaN/GaN MQW photoanode after reliability test 2 hours.

X-ray photoelectron spectroscopy (XPS) was carried out on the InGaN/GaN MQW photoanode s before and after PEC analysis, as shown in **Figure 6-b** (see **Figure S8** and **S9** in Supporting Information). For the bare InGaN/GaN MQW before PEC, as shown in **Figure 6a**, peaks were seen in the Ga 2p spectrum that were fitted with a simple doublet separated by 26.9 eV, with the Ga $2p_{3/2}$ transition centred at 1117.2 eV

and corresponding to Ga-N.[26] The N 1s spectrum showed an asymmetric broad peak with two distinct shoulders. A good fit was obtained by deconvoluting the experimental data using three peaks with a full width half maximum of 1.6-1.9 eV as suggested by Bertoti.[26] Doing so yielded a primary peak centred at 397.1 eV, corresponding to N-Ga.[26] The additional peaks at lower binding energies of 395.4 and 393.9 eV do not appear to match any N species, but this may be due to oxygen contamination (which was detected on the surface and in the bulk [data not shown], which is known to cause N 1s peaks to shifted in metal nitride films.[26] After PEC, XPS analysis of bare InGaN/GaN MQW showed the surface to have deteriorated, resulting in a much weaker signal for the Ga 2p transition than previously seen. The N 1s spectrum, when deconvoluted, showed a principle peak at 399.4 eV corresponding to surface organic nitrogen species. Additional peaks were seen at 396.4 and 394.4 eV, corresponding to N bound to Ga, and possibly N-In (respectively) as a weak signal for In 3d was also observed (see supporting information **Figure S8**).[27]

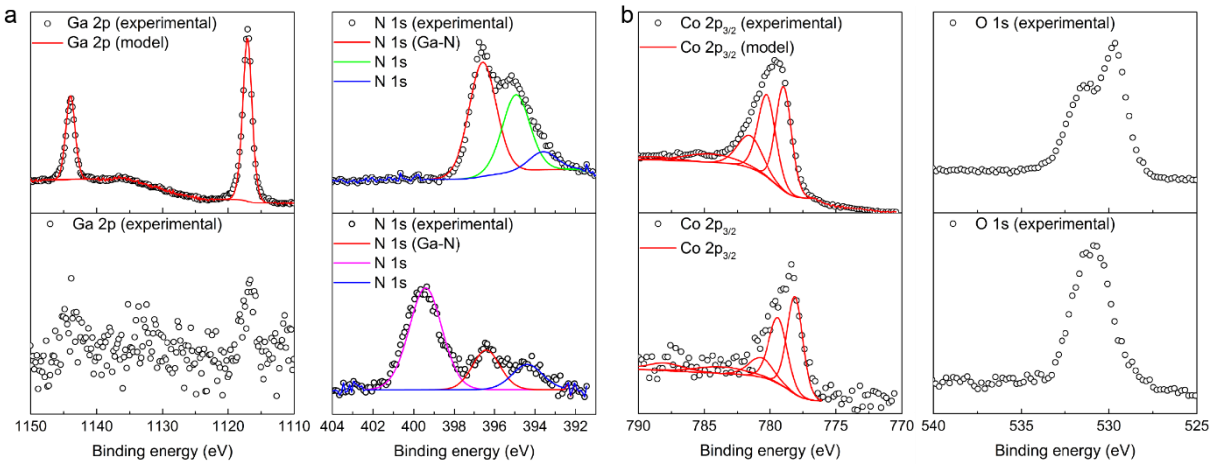

Figure 6. Chemical properties of both InGaN/GaN MQW photoanode s before and after PEC testing. (a) XPS spectra showing the surface composition of the InGaN/GaN MQW photoanode detailing of Ga and N transitions before and after reliability test 2 hours. **(b)** XPS spectra showing the surface composition of the InGaN/GaN MQW

modified with CoOx photoanode detailing of Co, and O before and after reliability test 28 hours.

For the InGaN/GaN MQW-CoO_x photoanode before PEC analysis, as shown in **Figure 6b**, XPS showed the immediate surface to be composed only of Co_3O_4, as expected due to the surface oxidation of CoO. The Co $2p_{3/2}$ transition was deconvoluted using five peaks according to the fitting parameters given by Biesinger et al.[28] After PEC analysis, the protective Co_3O_4/CoO layer was still present (as also observed via SEM). However, XPS peaks for In 3d, Ga 2p and N 1s were now also visible, suggesting that the Co_3O_4/CoO layer, though present, was partially deteriorated by the electrolyte solution during PEC (see supporting information **Figure S9**). The In 3d spectrum was a simple doublet, with the In $3d_{5/2}$ peak centred at 444.3 eV corresponding to In-N. The Ga 2p3/2 transition was centred at 1116.6 eV, which is within the range for Ga-N.[26] The nitrogen 1s spectrum showed four different environments, as explained before, with the most prominent peak at 396.5 eV and assigned to N bound to Ga.[26]

Conclusion

In conclusion, we demonstrate an InGaN/GaN MQW photoanode with improved efficiency and stability by coupling a cobalt oxide co-catalyst that is earth-abundant and highly active for oxidation evolution reaction. Cobalt oxide thin-film coating on the InGaN/GaN MQW photoanode significantly enhanced the stability up to 20 hr, maintaining > 50% of their initial photocurrent density, while the InGaN/GaN MQW without catalyst began to corrode in the first 30 min. Also, electrochemical impedance spectroscopy and surface characterisations showed InGaN/GaN MQW modified with CoO_x reduced the reaction resistance to some extent, thus providing enhanced photoelectrochemical efficiency and stability.

Experimental

Crystal Growth: The structure of InGaN/GaN MQW were grown heteroepitaxially by atmospheric pressure metal organic chemical vapour deposition (MOCVD) on (0001) patterned sapphire substrates (PSS). Prior to the deposition of the MQWs growth, a 3.5 µm unintentionally doped (UID) GaN template layer grown at 1200 °C followed by the active region consisted of an undoped eight periods multiple-quantum well (MQW that was grown in two steps: the first step consisted of the growth of a 3 nm InGaN QW with ~ 20 % indium content, followed immediately by the growth of a 2 nm GaN cap layer at the same temperature; the second step consisted of ramping up the temperature 100 °C higher than the QWs and the growth of a 8 nm high temperature (HT) GaN barrier. The growth rates of the InGaN QW, GaN cap layer and HT GaN barrier for the structure in this study were 1 Å/sec, 0.5 Å/sec and 0.35 Å/sec, respectively.

Atomic Layer Deposition: ALD was performed in a home-made closed chamber-type ALD reactor at 250 ^{o}C, using ultrahigh purity N_2 (99.999%) carrier gas at a flow rate of 50 sccm and a pressure of 60 Pa. The CoO_x layer (12 ~ 13 nm) was deposited onto the surface of InGaN/GaN MQWs by sequential exposure of the cobaltocene ($CoCp_2$, 75 ^{o}C) and O_3 with 350 cycles.[29,30] The pulse, exposure, and purge times were 5 s, 8 s, and 20 s for $CoCp_2$, and 0.1 s, 8 s, and 20 s for O_3, respectively.

Materials Characterisation: The high-resolution TEM (HRTEM) images and EELS spectra were obtained using a FEI Titan 80-300 KV microscope assembled with a spherical aberration corrector of the imaging lens, a monochromator, and a high-resolution spectrometer (Gatan Image Filter Tridiem 965). The microscope was operated at 80 kV, and the spectra were collected in STEM mode, which used the

spectrum imaging technique with 0.1 eV per channel dispersion of the spectrometer. The TEM sample was prepared by a Zeiss NVision 40 dual beam, focused ion beam/scanning electron microscope (FIB/SEM), and then the sample was sealed in a vacuum transfer holder (Gatan Model 648) for further TEM characterization and electron energy loss spectroscopy (EELS) analysis. The XRD measurement was performed by a Jordan Valley D1 X-ray diffraction instrument. Scanning electron microscope (SEM) analysis was carried out using a Hitachi S-4800 SEM at 3kV accelerating voltage. X-ray photoelectron spectroscopy (XPS) measurements were performed with a Thermo monochromated aluminium k-alfa photoelectron spectrometer, using monochromic Al-Kα radiation (1486.7 eV). Survey scans were collected in the range of 0 - 1300 eV. High resolution peaks were used for the principal peaks of Ga, As, Ti 2p and O 1s, Ni, Au. The area underneath these bands is an indication of the concentration of element within the region of analysis (spot size 400 μm). Data was analysed with CasaXPS software. Raman measurements were carried out in a Renishaw inVia micro-Raman system by 1800 g mm^{-2} grating through a ×50 objective lens and using a 532-nm excitation laser. The laser power was controlled at about 10%.

Device Fabrication: Before the PEC experiments, a window for a contact was patterned by typical lithography process and then was etched down to the GaN template by reactive ion etching. A metal of Ti/Au for ohmic contact was deposited on the GaN template with a thickness of 35 and 500 nm, respectively. Rapid thermal annealing (RTA) was performed at temperature of 850 °C for 30 s. Then, the sample was attached by a copper wire using silver paste and covered by insulating epoxy.

Photoelectrochemical Measurements: A 200W Xe arc lamp (66477-200HXF-R1 Mercury-Xenon) using as a light source with AM 1.5 G filter to produce simulated sunlight. The illumination intensity was calibrated using a silicon reference cell with a Power Meter (Thorlabs, Model PM100A). Before PEC experiments, the electrolyte was purged by Ar for 30 mins. PEC measurements were performed in a three-electrode configuration using photoanodes as working electrode, silver/silver chloride (Ag/AgCl) as a reference electrode and platinum coil as the counter electrode in 1 M NaOH pH ~ 13.7 in single compartment PEC cell with quartz window. The measured potentials vs. the Ag/AgCl were converted to the reversible hydrogen electrode (RHE) scale using the following Nernst Equation:

$$\mathrm{V_{RHE}} = \mathrm{V_{Ag/AgCl}} + 0.059 \times \mathrm{PH} + \mathrm{V^{0}_{Ag/AgCl}} \quad (1)$$

Where $\mathrm{V_{Ag/AgCl}}$ the potential is experimentally measured vs. Ag/AgCl reference electrode, and $\mathrm{V^{0}_{Ag/AgCl}}$ is the standard potential of Ag/AgCl at 25 °C (0.1976 V vs. RHE). All linear sweep voltammetry measurements with a scan rate of 50 mV s^{-1} was performed under both dark and illumination conditions using a potentiostat (Ivium CompactStat).

The IPCE defines the ratio of the number of photogenerated electrons engaged in the reaction over the number of incident photons at a certain wavelength. It can be computed by using the following equation.

$$\mathrm{IPCE} = \frac{1239.8\ (V\ nm) \times [\ J\ (mAcm^{-2})\ ]}{P_{mono}\ (mW\ cm^{-2}) \times \lambda\ (nm)} \quad (2)$$

Where J is the photocurrent density, P_{mono} is the monochromated illumination power intensity and λ the wavelength. The photocurrent was obtained by subtracting the dark current from the light current. The ABPE was measured from the following equation.

$$ABPE = \left[\frac{J_{ph}\left(mA\ cm^{-2}\right) \times (1.23 - V_b)(V) \times \eta_{\mathcal{F}}}{P_{total}\ (mW/cm^2}\right] \quad (3)$$

Where J is the photocurrent density, P the incident illumination intensity (100 mW cm^{-2}), V_b the potential versus counter electrode, $\eta_{\mathcal{F}}$ faradaic efficiency.

The overall solar-to-hydrogen conversion efficiency (STH) is calculated as

$$STH = \left[\frac{J_{SC}\ \left(mA\ cm^{-2}\right) \times (1.23\ V) \times \eta_{\mathcal{F}}}{P_{total}\ (mW/cm^2}\right] \quad (4)$$

Where J_{SC} is the short-circuit photocurrent density, 1.23V corresponds to the Gibbs free energy (ΔG) of the reaction, and $\eta_{\mathcal{F}}$ is faradaic efficiency.

AUTHOR INFORMATION

Corresponding Authors

E-mail: mahdi.alqahtani.16@ucl.ac.uk
E-mail: huiyun.liu@ucl.ac.uk
E-mail: jiang.wu@ucl.ac.uk

Author contributions

M.A. and J.W. conceived the idea. A.A. and S.N grew the InGaN/GaN MQW structure by MOCVD. M.A. performed the PEC experiments and analysed the data. I.P. and S.S. performed XPS and related analysis. S.B.J performed Raman measurements. M.A and J.W. analysed the STEM and EDX mapping. F.C. and S.S performed SEM and

related analysis. B.Z. and Y.Q. performed ALD CoO_x. M.A. and J.W wrote the manuscript. All authors reviewed and commented on the manuscript.

Notes

The authors declare no competing financial interest.

Acknowledgements

This work is being supported by EPSRC grant EP/P006973/1 and King Abdulaziz City for Science and Technology (KACST), Riyadh, Saudi Arabia. Mahdi Alqahtani acknowledges the financial support from the King Abdulaziz City for Science and Technology (KACST) scholarship program.

References

1 Pinaud, B. A. *et al.* Technical and economic feasibility of centralized facilities for solar hydrogen production via photocatalysis and photoelectrochemistry. *Energy Environ. Sci.* **6**, 1983-2002, doi:10.1039/c3ee40831k (2013).

2 Lewis, N. S. & Nocera, D. G. Powering the planet: chemical challenges in solar energy utilization. *Proc. Natl. Acad. Sci. U. S. A.* **103**, 15729-15735, doi:10.1073/pnas.0603395103 (2006).

3 Bard, A. J. Photoelectrochemistry. *Science* **207**, 139-144, doi:10.1126/science.207.4427.139 (1980).

4 Turne, J. A. Sustainable Hydrogen Production. *Science* **305**, 972-974, doi:0.1126/science.1103197 (2004).

5 Fujishima, A. & Honda, K. Electrochemical Photolysis of Water at a Semiconductor Electrode. *Nature* **238**, 37-38, doi:10.1038/238037a0 (1972).

6 Hettick, M. *et al.* Nonepitaxial Thin-Film InP for Scalable and Efficient Photocathodes. *J. Phys. Chem. Lett.* **6**, 2177-2182, doi:10.1021/acs.jpclett.5b00744 (2015).

7 Wu, J. *et al.* Wafer-scale fabrication of self-catalyzed 1.7 eV GaAsP core-shell nanowire photocathode on silicon substrates. *Nano Lett.* **14**, 2013-2018, doi:10.1021/nl500170m (2014).

8 Hu, S. *et al.* Amorphous TiO(2) coatings stabilize Si, GaAs, and GaP photoanodes for efficient water oxidation. *Science* **344**, 1005-1009, doi:10.1126/science.1251428 (2014).

9 McCrory, C. C., Jung, S., Peters, J. C. & Jaramillo, T. F. Benchmarking heterogeneous electrocatalysts for the oxygen evolution reaction. *J. Am. Chem. Soc.* **135**, 16977-16987, doi:10.1021/ja407115p (2013).

10 Stampfl, C. & Van de Walle, C. G. Energetics and electronic structure of stacking faults in AlN, GaN, and InN. *Phys. Rev. B* **57**, R15052-R15055, doi:10.1103/PhysRevB.57.R15052 (1998).

11 Moses, P. G. & Van de Walle, C. G. Band bowing and band alignment in InGaN alloys. *Appl. Phys. Lett.* **96**, 021908, doi:10.1063/1.3291055 (2010).

12 Nakamura, S. The roles of structural imperfections in InGaN-based blue light-emitting diodes and laser diodes. *Science* **281**, 955-961 (1998).

13 Neuderth, P. *et al.* Passivation layers for nanostructured photoanodes: ultra-thin oxides on InGaN nanowires. *J. Mater. Chem. A* **6**, 565-573, doi:10.1039/c7ta08071a (2018).

14 Caccamo, L. *et al.* Insights into Interfacial Changes and Photoelectrochemical Stability of In(x)Ga(1-x)N (0001) Photoanode Surfaces in Liquid Environments. *ACS Appl Mater Interfaces* **8**, 8232-8238, doi:10.1021/acsami.5b12583 (2016).

15 AlOtaibi, B. *et al.* Highly stable photoelectrochemical water splitting and hydrogen generation using a double-band InGaN/GaN core/shell nanowire photoanode. *Nano Lett* **13**, 4356-4361, doi:10.1021/nl402156e (2013).

16 JumpeiKamimura, † PeterBogdanoff,‡FatwaF.Abdi,‡ JonasLahnemann,†RoelvandeKrol,‡ Henning Riechert,† and Lutz Geelhaar†. Photoelectrochemical Properties of GaN Photoanodes with Cobalt Phosphate Catalyst for Solar Water Splitting in Neutral Electrolyte. *J. Phys. Chem. C*, doi:10.1021/acs.jpcc.7b02253 (2017).

17 Ebaid, M. *et al.* Unbiased photocatalytic hydrogen generation from pure water on stable Ir-treated In 0.33 Ga 0.67 N nanorods. *Nano Energy* **37**, 158-167, doi:10.1016/j.nanoen.2017.05.013 (2017).

18 Chu, S. *et al.* Solar Water Oxidation by an InGaN Nanowire Photoanode with a Bandgap of 1.7 eV. *ACS Energy Lett.* **3**, 307-314, doi:10.1021/acsenergylett.7b01138 (2018).

19 Liu, G. *et al.* Robust Sub-Monolayers of Co3O4Nano-Islands: A Highly Transparent Morphology for Efficient Water Oxidation Catalysis. *Advanced Energy Materials* **6**, doi:10.1002/aenm.201600697 (2016).

20 Alhassan, A. I. *et al.* High luminous efficacy green light-emitting diodes with AlGaN cap layer. *Opt. Express* **24**, 17868-17873, doi:10.1364/OE.24.017868 (2016).

21 Bae, D., Seger, B., Vesborg, P. C., Hansen, O. & Chorkendorff, I. Strategies for stable water splitting via protected photoelectrodes. *Chem. Soc. Rev.* **46**, 1933-1954, doi:10.1039/c6cs00918b (2017).

22 Lichterman, M. F. *et al.* Enhanced Stability and Activity for Water Oxidation in Alkaline Media with Bismuth Vanadate Photoelectrodes Modified with a Cobalt Oxide Catalytic Layer Produced by Atomic Layer Deposition. *The Journal of Physical Chemistry Letters* **4**, 4188-4191, doi:10.1021/jz4022415 (2013).

23 Yang, J. *et al.* Efficient and sustained photoelectrochemical water oxidation by cobalt oxide/silicon photoanodes with nanotextured interfaces. *J Am Chem Soc* **136**, 6191-6194, doi:10.1021/ja501513t (2014).

24 Mishra, P. *et al.* On the optical and microstrain analysis of graded InGaN/GaN MQWs based on plasma assisted molecular beam epitaxy. *Opt. Mater. Express* **6**, 2052-2062, doi:10.1364/ome.6.002052 (2016).

25 Bae, D., Seger, B., Vesborg, P. C., Hansen, O. & Chorkendorff, I. Strategies for stable water splitting via protected photoelectrodes. *Chem Soc Rev* **46**, 1933-1954, doi:10.1039/c6cs00918b (2017).

26 Bertóti, I. Characterization of nitride coatings by XPS. *Surf. Coat. Technol.* **151-152**, 194-203, doi:10.1016/s0257-8972(01)01619-x (2002).

27 Guo, Q. X., Nishio, M., Ogawa, H., Wakahara, A. & Yoshida, A. Electronic structure of indium nitride studied by photoelectron spectroscopy. *Phys. Rev. B* **58**, 15304-15306, doi:10.1103/PhysRevB.58.15304 (1998).

28 Biesinger, M. C. *et al.* Resolving surface chemical states in XPS analysis of first row transition metals, oxides and hydroxides: Cr, Mn, Fe, Co and Ni. *Appl. Surf. Sci.* **257**, 2717-2730, doi:10.1016/j.apsusc.2010.10.051 (2011).

29 Zhang, J. *et al.* Porous TiO2 Nanotubes with Spatially Separated Platinum and CoOx Cocatalysts Produced by Atomic Layer Deposition for Photocatalytic Hydrogen

Production. *Angew. Chem. Int. Ed. Engl.* **56**, 816-820, doi:10.1002/anie.201611137 (2017).

30 Li, Y. Q. *et al.* Highly efficient CoOx/SBA-15 catalysts prepared by atomic layer deposition for the epoxidation reaction of styrene. *Catal.: Sci. Technol.* **7**, 2032-2038, doi:10.1039/c7cy00349h (2017).